ELSEVIER

Journal of Alloys and Compounds 444–445 (2007) 457–463

Journal of ALLOYS AND COMPOUNDS

www.elsevier.com/locate/jallcom

Nanostructured actinide compounds

Sergey V. Krivovichev [a,b,*], Peter C. Burns [c], Ivan G. Tananaev [b], Boris F. Myasoedov [b]

[a] *Department of Crystallography, Faculty of Geology, St.Petersburg State University, University Emb. 7/9, 199034 St.Petersburg, Russia*
[b] *A.N. Frumkin Institute of Physical Chemistry and Electrochemistry, Russian Academy of Sciences, Leninsky pr. 31, Moscow 119991, Russia*
[c] *Department of Civil Engineering and Geological Sciences, University of Notre Dame, Notre Dame, IN 46556-0767, USA*

Received 5 September 2006; received in revised form 29 September 2006; accepted 4 October 2006
Available online 21 November 2006

Abstract

A brief overview of nanostructured inorganic actinide compounds, i.e., compounds with nanoscale clusters and structural units, is given. Only structures that are accessible via X-ray diffraction analysis are considered (i.e., highly ordered assemblies of molecular units with at least one dimension of more than 1 nm). Zero-dimensional (0D) actinide based nanostructures are represented by a new family of self-assembling actinide nanospheres recently reported by Burns et al. [P.C. Burns, K.-A. Hughes Kubatko, G. Sigmon, B.J. Fryer, J.E. Gagnon, M.R. Antonio, L. Soderholm, Angew. Chem. Int. Ed. 44 (2005) 2135]. The nanospheres are comprised of linear actinyl-peroxide building blocks, and their persistence as stable entities in alkaline solutions has been confirmed. Krivovichev et al. [S.V. Krivovichev, V. Kahlenberg, R. Kaindl, E. Mersdorf, I.G. Tananaev, B.F. Myasoedov, Angew. Chem. Int. Ed. 44 (2005) 1134; J. Am. Chem. Soc. 127 (2005) 1072] have recently reported synthesis and structures of two uranium(VI) compounds, $K_5[(UO_2)_3(SeO_4)_5](NO_3)(H_2O)_{3.5}$ (**1**) and $(C_4H_{12}N)_{14}$ $[(UO_2)_{10}(SeO_4)_{17}(H_2O)]$ (**2**), containing nanometer-sized tubules formed by corner sharing of $U^{6+}O_7$ pentagonal bipyramids and SeO_4 tetrahedra. Actinide peroxide nanospheres and uranyl selenate nanotubules represent the first examples of nanoscale structures in inorganic actinide compounds. These findings demonstrate the possibility of nanoscale fabrication for actinides in higher oxidation states, and a whole new range of uranium-based nanotubular and nanocomposite materials can be expected.

Keywords: Nanostructures; Nanospheres; Nanotubules; Uranium; Neptunium

1. Introduction

Nanomaterials consist of a range of structures with at least one dimension in the nanometer range (1–1000 nm). These include nanocrystals and clusters (quantum dots), nanowires, nanotubes, thin films and superlattices (three-dimensional (3D) structures) [1,2]. Usually, nanostructures have more reactive surfaces and exhibit new functions relative to macroscopic materials of the same chemical composition. Investigations of the organization of matter at the nano-level are under way in many chemical systems with present and potential applications in nanotechnology. Recently, nanoscale structures were reported for the first time for actinide-containing compounds [3–6].

Here we provide a brief overview of nanostructured inorganic actinide compounds, i.e., compounds with nanoscale clusters and structural units. At present, we discuss only those structures that are accessible via X-ray diffraction analysis, i.e., highly ordered assemblies of units with at least dimension of more than 1 nm. This imposes certain limits on the range of objects under consideration; however, it provides the fine-scale details of structural geometry and topology (bond lengths, bond and torsion angles, intermolecular interactions, etc.). The latter is important in elaborating the principles of structural organization and self-assembly of actinide nanoclusters on the basis of precise measurements of structural parameters.

It is well-known that the solid-state chemistry of inorganic oxocompounds of hexa-, penta- and heptavalent actinide ions (An) is dominated by 2-dimensional (2D) layered structures, due to the strong tendency of An^{m+} cations ($m = 5$–7) to form linear actinyl ions, $AnO_2^{(m-4)+}$ [7,8]. The 2D nature of polyhedral polymerization makes actinide oxocompounds attractive from the viewpoint of their potential to form nanostructures based upon real-2D and pseudo-2D topologies. For instance, spontaneous formation of nanotubes was observed in a number

* Corresponding author. Tel.: +812 3289647.
E-mail address: skrivovi@mail.ru (S.V. Krivovichev).

0925-8388/$ – see front matter © 2006 Published by Elsevier B.V.
doi:10.1016/j.jallcom.2006.10.077

of systems where exfoliation of lamellar solids into individual sheets can be achieved [9].

2. Zero-dimensional (0D) structures: actinide peroxide nanospheres

Self-assembling clusters have received considerable attention because they are excellent venues for the study of structure-property relationships. Monodisperse nanoaggregates have been reported with various compositions, including C-60-buckminsterfullerene and transition-metal oxide clusters. Numerous polyoxometalates have been synthesized and described that are built from WO, MoO, and NbO framework structures [10]. Small clusters provide important insights concerning the influence of the nanoscale on electronic, magnetic, and structural properties [11,12]. Nanoparticles are also important in environmental systems [13]. Recently, Burns et al. [3] reported the synthesis and characterization of a new family of self-assembling actinide nanospheres with compositions such as $K_{16}(H_2O)_2(UO_2)(O_2)_2(H_2O)_2[(UO_2)(O_2)_{1.5}]_{28}$ and $Li_6(H_2O)_8NpO_2(H_2O)_4[(NpO_2)(O_2)(OH)]_{24}$ that are comprised of linear actinyl-peroxide building blocks, and their persistence as stable entities in alkaline solutions.

The structures of the nanoclusters were obtained by crystallizing them into molecular crystals, followed by structural analysis using single-crystal X-ray diffraction (Table 1). Once the details of the structures were obtained, their presence in alkaline solutions was verified using small angle X-ray scattering at the Advanced Photon Source in Chicago. The nanospheres shown in Fig. 1 contain 24 (U-24, Np-24, Fig. 1a), 28 (U-28, Fig. 1b) and 32 (U-32, Fig. 1c) actinyl polyhedra. The nanoclusters are comprised of two types of actinyl peroxide polyhedra. U-24, U-32 and Np-24 contain locally identical $(AnO_2)(O_2^{2-})_2(OH)_2$ hexagonal bipyramids, with O atoms of the actinyl ions constituting apices of the bipyramids, and peroxide groups form two of the equatorial edges of the polyhedra. U-28 contains only $(AnO_2)(O_2^{2-})_3$ hexagonal bipyramids, in which three equatorial edges of the polyhedra are peroxide groups. In all cases, hexagonal bipyramids link by sharing three of their equatorial edges with adjacent polyhedra. In U-24, Np-24 and U-32, two of the shared edges correspond to peroxide groups, whereas the third edge consists of two hydroxyl groups. In U-28, all three shared edges are peroxide groups. Outer surfaces of the nanospheres are O atoms of the actinyl ions, which can only accept weak bonds.

Table 1
Crystallographic parameters of actinyl peroxides containing peroxide nanospheres

Name	Space groups	a (Å)/α (°)	b (Å)/β (°)	c (Å)/γ (°)
U-24	$P\bar{1}$	19.211/102.40	31.003/99.50	32.252/95.36
Np-24	$I4/m$	18.155/90	18.155/90	26.693/90
U-28	$Pbcm$	19.261/90	33.813/90	28.163/90
U-32	$P2_1/c$	38.84/90	36.52/102.86	41.30/90

Fig. 2 shows the linkage of polyhedra into four-membered rings that occur in the structures of U-24, U-32 and Np-24. Each shared edge within the four-membered ring is peroxide, with lengths of ~1.45 Å, whereas the edge defined by one O atom of each of the two peroxide groups is ~2.8 Å. Linkage of four polyhedra into a ring can only be accomplished if the polyhedra are significantly tilted, such that the actinyl ions are directed towards a common point located ~3.5 Å below the four co-planar actinide cations (Fig. 2c). The linkage of eight identical four-membered rings of polyhedra results in the nanosphere found in U-24 and Np-24 (Fig. 2d).

The topology and symmetry of the actinide peroxide nanospheres requires special attention. Fig. 1d–f show graphical

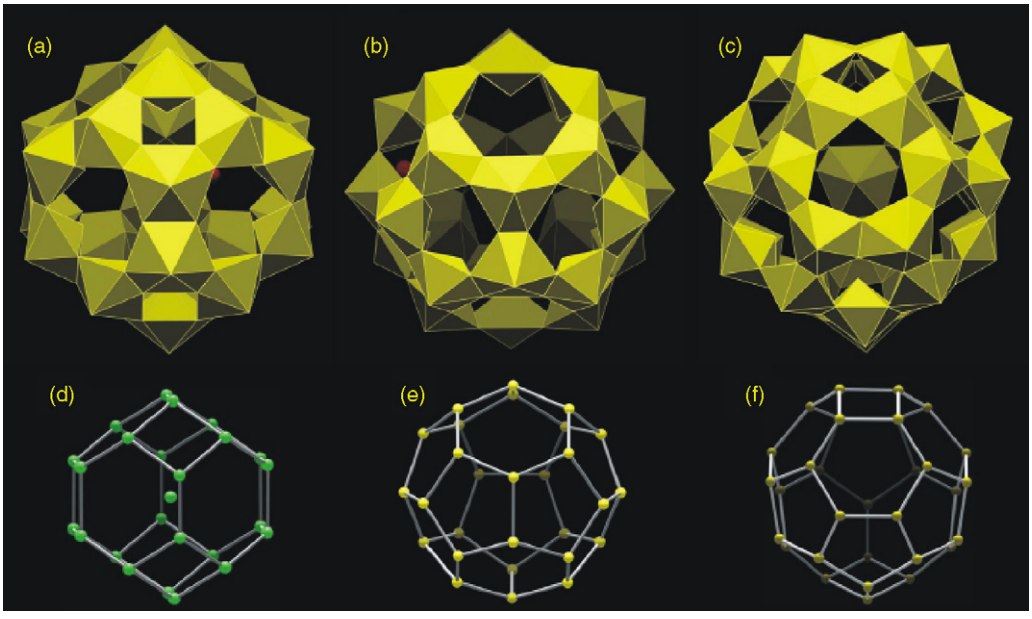

Fig. 1. Polyhedral representations of spherical actinyl peroxide nanoclusters found in U-24 and Np-24 (a), U-28 (b), and U-32 (c). An–An connectivity diagrams for Np-24, U-28, and U-32 are in (d–f), respectively.

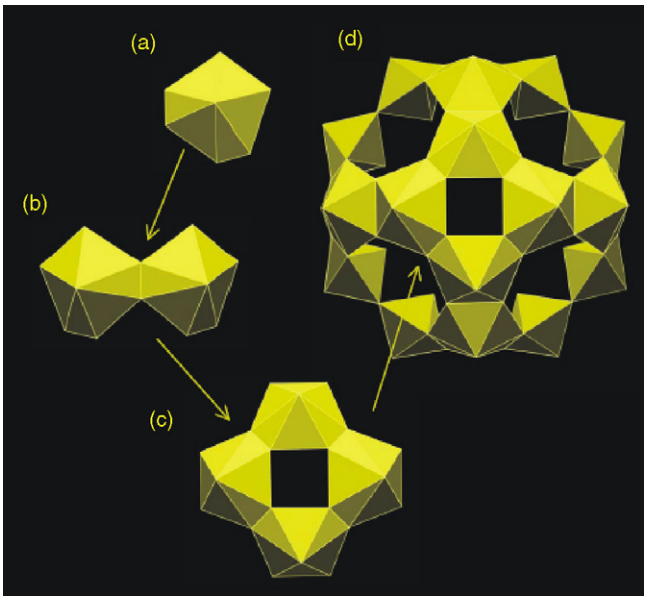

Fig. 2. Polyhedral representations of linkages in the U-24 and Np-24 nanoclusters. (a) hexagonal bipyramid with composition $(AnO_2)(O_2)_2(OH)_2$. (b) Linkages of two hexagonal bipyramids by the sharing of a peroxide edge. (c) Linkage of four hexagonal bipyramids into a four-membered ring by the sharing of four peroxide edges. (d) U-24 cluster.

descriptions of the nanospheres where all An centers are replaced by nodes and nodes are linked if respective U atoms have common ligands. This kind of presentation is especially convenient for the investigation of topological properties of polyhedral clusters. One can apply all topological tools that are typically used for the description of the topology of convex polytopes [14].

The *face symbol* is the number of polygonal faces comprising the polyhedron specified by the number of their vertices; for instance, the face symbol for a cube is 4^6 [it has 6 (superscript) square faces]. Face symbols for the clusters shown in Fig. 1 are 4^66^8, $5^{12}6^4$ and $4^25^86^8$, for U-24, U-28 and U-32, respectively.

A *valency* of a vertex in a graph is the number of edges incident upon it. Analysis of polyhedral diagrams in Fig. 1 shows that all vertices in the clusters are trivalent, i.e., each An center is linked to three adjacent An centers in each cluster.

The *Steiniz theorem* (in its simplified formulation) states that a net of edges and vertices of a 3D polyhedron can be projected onto 2D plane without the intersections of edges. The resulting projection is a *Schlegel projection* or *Schlegel diagram*. These diagrams were first used in crystal chemistry by Moore [15] to compare the geometries of coordination polyhedra in basic iron phosphates. Later, they were recognized as an important tool for the study of structural topologies and geometries by Hoppe and Köhler [16], Dvoncova and Lii [17], and Krivovichev et al. [18]. Currently, they are actively used in discussions of isomerization and topological transformations of carbon clusters, fullerenes and metallofullerenes [19,20]. Schlegel diagrams of actinide peroxide nanospheres are shown in Fig. 3. Whereas the U-24 and Np-24 clusters are easily recognized as cubooctahedra with an ideal symmetry $m3m$, the U-28 and U-32 clusters are more complex. In its ideal $m3m$-version, the U-24 cluster has all its vertices as symmetry-equivalent. In contrast, vertices of the U-28 cluster belong to two symmetry non-equivalent classes, and the ideal symmetry is $\bar{4}3m$. It is remarkable that the cluster U-32 has a non-crystallographic point group $\bar{8}2m$ with eight-fold inversion symmetry axis running through the centers of opposite four-membered rings. The U-32 cluster has three classes of non-equivalent vertices (Fig. 3).

3. One-dimensional (1D) structures: uranyl selenate nanotubules

Since the discovery of carbon nanotubes in 1991 [21], a great deal of attention has focused on inorganic nanotubes as promising modules for nanotechnology applications. Oxidic nanotubes are of special interest because of their unique atomic structure and interesting physical properties [22,23]. Krivovichev et al. [4,5] have recently reported synthesis and structures of two uranium(VI) compounds, $K_5[(UO_2)_3(SeO_4)_5](NO_3)(H_2O)_{3.5}$ (**1**) and $(C_4H_{12}N)_{14}$ $[(UO_2)_{10}(SeO_4)_{17}(H_2O)]$ (**2**), containing nanometer-sized tubules formed by corner sharing of $U^{6+}O_7$ pentagonal bipyramids and SeO_4 tetrahedra [4,5].

The most intriguing feature of the structures of compounds **1** and **2** is that they contain isolated porous nanotubules formed by corner sharing of $U^{6+}O_7$ pentagonal bipyramids and SeO_4 tetrahedra (Fig. 4a). Such nanometer-scale tubules formed by

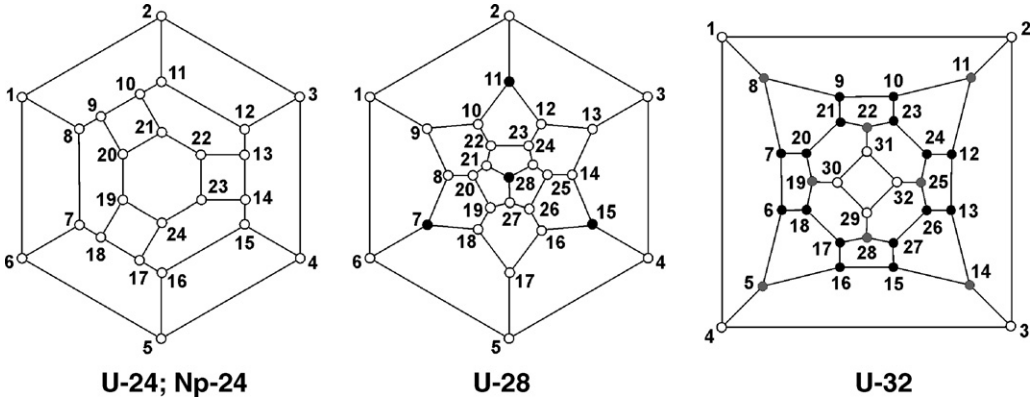

Fig. 3. Schlegel diagrams for the actinide peroxide nanospheres. Non-equivalent vertices are colored with different colors.

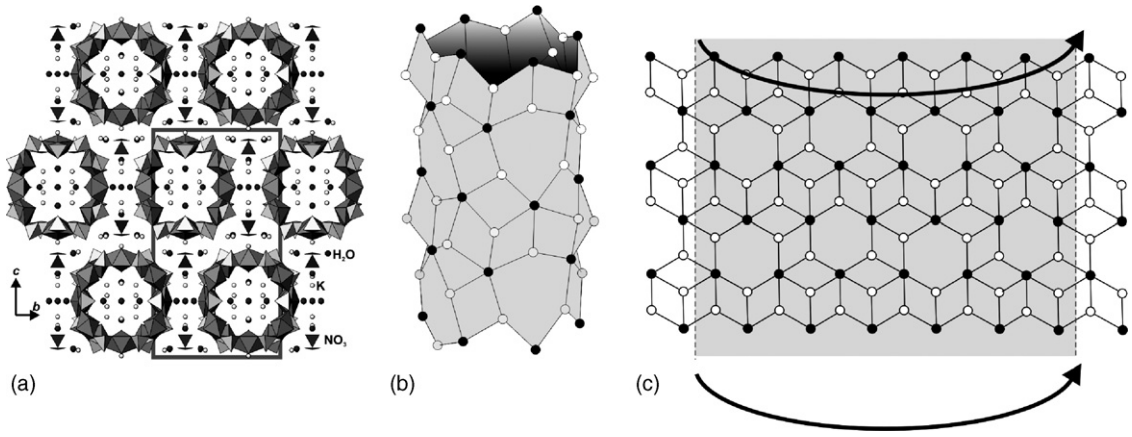

Fig. 4. The crystal structure of **1** projected along the *a* axis (a), tubular graph describing topology of the uranyl selenate nanotubule in **1** (b) and its unfolded version (c).

two types of coordination polyhedra are new in the realm of inorganic oxosalts; probably, the most closely related but yet distinct are elliptic porous nanorods in the structure of yuksporite, a natural material from the Kola peninsula, Russia [24]. The uranyl selenate nanotubules in the structures of **1** and **2** have circular cross-sections with outer diameters of 17 and ~25 Å (= 1.7 and 2.5 nm), respectively. The crystallographic free diameters of the tubules are 4.7 and 12.7 Å for **1** and **2**, respectively.

The topology of the uranyl selenate nanoscale tubules can be described by means of a graphical approach first suggested by Krivovichev and Burns [25] for analysis of structural topologies in uranyl molybdates. The $[UO_7]^{8-}$ bipyramids and $[SeO_4]^{2-}$ tetrahedra are symbolized by black and white vertices, respectively. The black-and-white graph corresponding to the topological structure of the $[(UO_2)_3(SeO_4)_5]^{4-}$ tubule in **1** is shown in Fig. 4b. Its idealized unfolded version is given in Fig. 4c. To obtain the tubular graph corresponding to the $[(UO_2)_3(SeO_4)_5]^{4-}$ tubule, one has to cut the graph into tapes along the lines indicated in Fig. 1c, to fold the tape and to glue its corresponding sides. The same procedure can be used to investigate the local topology of the tubules observed in the structure of **2**. The black-and-white graph corresponding to the topological structure of the $[(UO_2)_{10}(SeO_4)_{17}(H_2O)]^{14-}$ tubule in **2** is shown in Fig. 5a. Its idealized unfolded version is given in Fig. 5b. To obtain the tubular graph corresponding to the tubule shown in Fig. 5a, one has to cut the graph into tapes along the lines indicated in Fig. 5b, to fold the tape and to glue its sides.

Most of the known inorganic nanotubes have a prototype lamellar material from which they can be (at least theoretically) obtained by exfoliation and folding of single-layer sheets into a tube. The same holds for the uranyl selenate tubules observed in **1**. The 3:5 graph shown in Fig. 4b is an underlying topology for the $[(UO_2)_3(TO_4)_5]^{4-}$ sheets found in the structures of inorganic oxosalts with T = S, Cr, Se [26–30]. However, there are some complications that arise due to the richness of isomeric variations in this class of 2D units.

Fig. 6a and b shows the $[(UO_2)_3(CrO_4)_5]$ sheets observed in the structures of $Mg_2[(UO_2)_3(CrO_4)_5](H_2O)_{17}$ and $Ca_2[(UO_2)_3(CrO_4)_5](H_2O)_{19}$, respectively. These sheets are built up by corner sharing between UO_7 pentagonal bipyramids and CrO_4 tetrahedra. The topology of these sheets correspond to the same graph depicted in Fig. 6c. Yet, detailed analysis of the polyhedral diagrams shown in Fig. 6a and b shows that these two sheets cannot be transformed one into another without breaking of chemical bonds. This is because the orientation of chromate tetrahedra within the sheets is different. Each tetrahedron corresponds to a three-connected white vertex, such that three of its corners are shared with adjacent UO_7 pentagonal bipyramids. The fourth corner is not shared and it is oriented either up or down relative to the plane of the sheet. Fig. 6c shows a black-

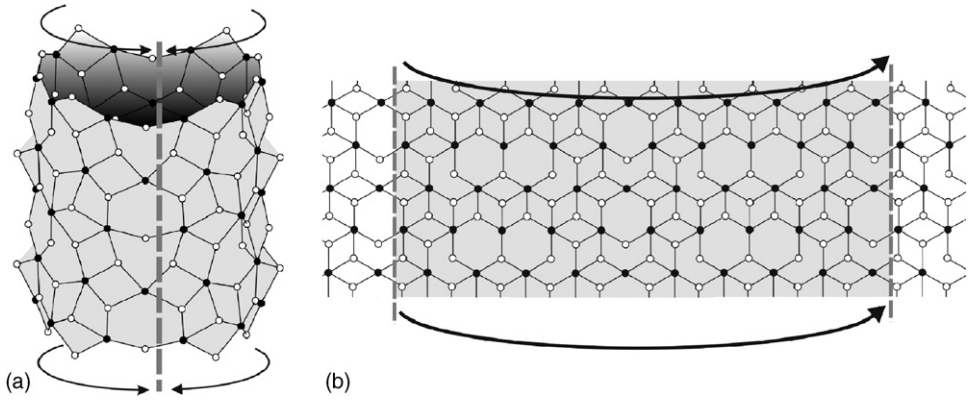

Fig. 5. Tubular graph describing topology of the uranyl selenate nanotubule in **2** (a) and its unfolded version (b).

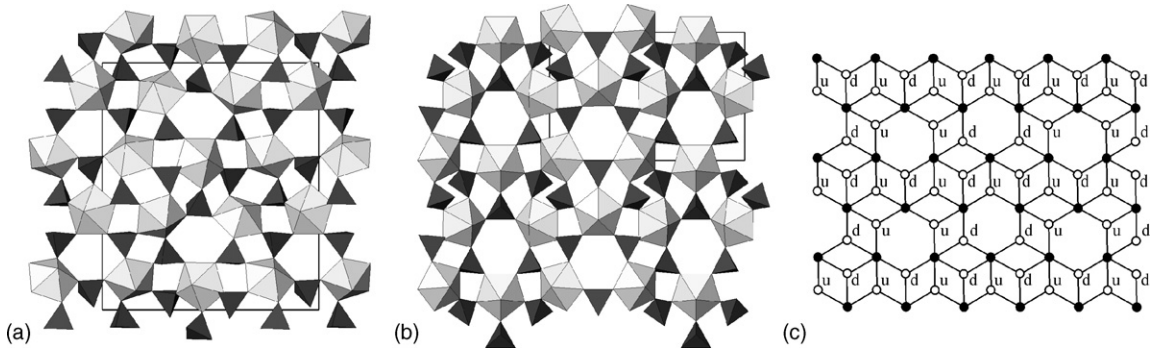

Fig. 6. The $[(UO_2)_3(CrO_4)_5]$ sheets observed in the structures of $Mg_2[(UO_2)_3(CrO_4)_5](H_2O)_{17}$ and $Ca_2[(UO_2)_3(CrO_4)_5](H_2O)_{19}$ (a and b, respectively) and the idealized topological structure of the latter (c).

and-white graph corresponding to the $[(UO_2)_3(CrO_4)_5]$ sheet in $Ca_2[(UO_2)_3(CrO_4)_5](H_2O)_{19}$, with the letters **u** and **d** written near the white nodes. The **u** and **d** designations indicate that the chromate tetrahedra symbolized by the white nodes have their non-shared corners oriented up or down relative to the plane of the sheet, respectively.

It is easy to calculate that the numbers of the **u** and **d** orientations in the $[(UO_2)_3(CrO_4)_5]$ sheets are the same; and this is true for other uranyl oxysalts as well (for uranyl selenates see refs. [26,27,31]). However, if one performs the same calculations for the selenate tetrahedra forming nanotubules in the structure of **1**, the obtained **u:d** ratio is 4:1 (here **u** orientations are those pointing *outside* a tubule). Thus, only one out of five tetrahedra is oriented inside the tubule. The possible reason is the tendency of the tubule to contain as much additional species (e.g., cations) as possible that results in a lower negative charge of the 'filled' tube.

The 10:17 graph of **2** shown in Fig. 5b has not been observed previously as an underlying topology for any inorganic compound. However, some parts of it are topologically isomorphous to the U:Se = 3:5 topology recently found in the structures of $Rb_4[(UO_2)_3(SeO_4)_5(H_2O)]$ [31], $[C_5H_{14}N]_4[(UO_2)_3(SeO_4)_4(HSeO_3)(H_2O)](H_2SeO_3)(HSeO_4)$ [32], $(H_3O)[C_5H_{14}N]_2[(UO_2)_3(SeO_4)_4(HSeO_4)(H_2O)]$ and $(H_3O)[C_5H_{14}N]_2[(UO_2)_3(SeO_4)_4(HSeO_4)(H_2O)](H_2O)$ [33].

The mechanism of formation of uranyl selenate tubules in aqueous media is probably controlled for compound **2** by the presence of protonated butylamine $(C_4H_{12}N)^+$ cations. In this regard, it can be similar to the process that leads to the formation of highly undulated uranyl selenate sheets in the structure of $(H_3O)_2[C_{12}H_{30}N_2]_3[(UO_2)_4(SeO_4)_8](H_2O)_5$ [34] (Fig. 7). Here the inorganic substructure consists of the UO_7 bipyramids and SeO_4^{2-} tetrahedra that share corners to form $[(UO_2)(SeO_4)_2]^{2-}$ sheets depicted in Fig. 8a. The sheets are parallel to (0 0 1) and are strongly undulated along the *c* axis. The undulation vector is parallel to [0 1 0] and equals to $b = 24.804$ Å. The undulation amplitude is about 25 Å. The undulations in the adjacent sheets have an anti-phase character so the large eliptical channels are created along the *a* axis. The organic substructure consists of micelles of protonated 1,12-dodecanediamine molecules oriented parallel to the *a* axis. The micelles occupy channels created by the packing of the $[(UO_2)(SeO_4)_2]^{2-}$ sheets.

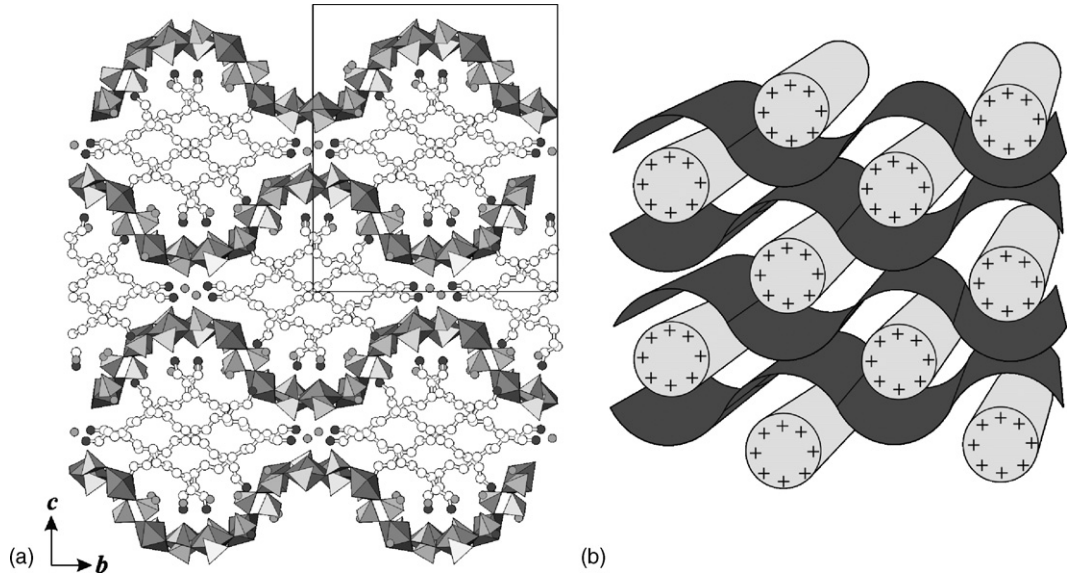

Fig. 7. Crystal structure of $(H_3O)_2[C_{12}H_{30}N_2]_3[(UO_2)_4(SeO_4)_8]\,(H_2O)_5$ (a) and a scheme of its construction ((b) inorganic layers are dark, organic micelles are light).

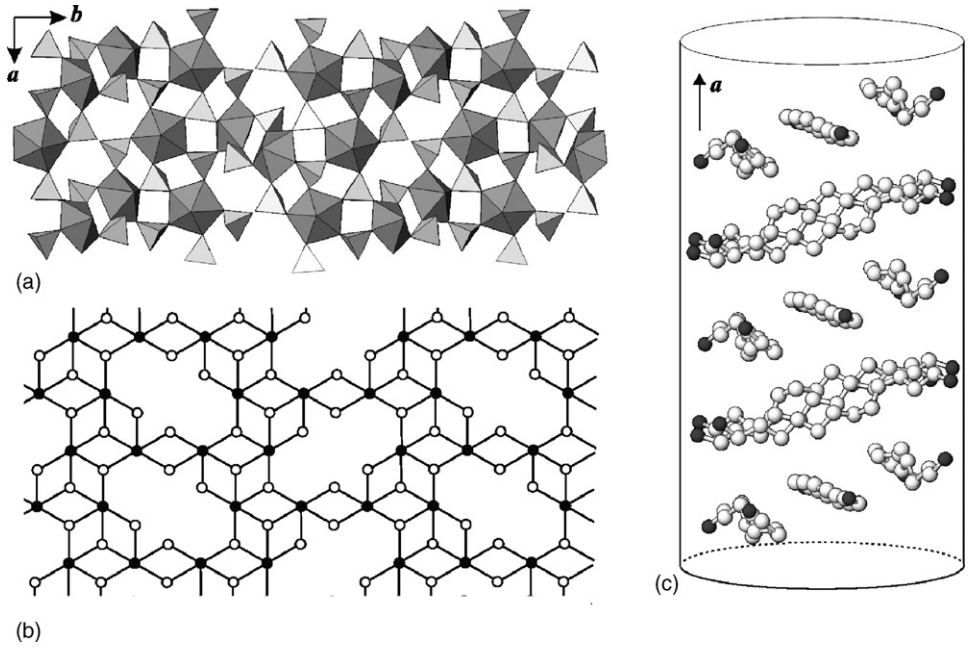

Fig. 8. The $[(UO_2)(SeO_4)_2]^{2-}$ sheet in the structure of $(H_3O)_2[C_{12}H_{30}N_2]_3[(UO_2)_4(SeO_4)_8](H_2O)_5$ (a), its nodal representation (U and Se polyhedra are symbolized by black and white circles, respectively) (b), and organization of 1,12-dodecanediamine molecules into a micelle (c).

The scheme of assembly of the 1,12-dodecanediamine chain molecules within the micelle is shown in Fig. 8c. The molecules are arranged into sublayers approximately parallel to (−102). The planes of these sublayers are not perpendicular to the micelle axis but form an angle of about 60°. In each layer, there are three $[C_{12}H_{30}N_2]^{2+}$ molecules that are parallel to each other. The molecules in the adjacent layers are at a 30° angle relative to each other, and this results in the elliptical form of the perpendicular section of the micelle. The lateral dimensions of the micelle are about 20 × 24 Å, i.e., are on the scale of nanometers. The interactions between organic and inorganic substructures involve N···O hydrogen bonds to oxygen atoms of uranyl ions and terminal oxygen atoms of selenate tetrahedra.

The protonated amine molecules with long-chain structure are known to form cylindrical micelles in aqueous solutions that involve self-assembly governed by competing hydrophobic/hydrophillic interactions. The flexible inorganic complexes present in the reaction mixture could then form around cylindrical micelles to produce an inorganic structure that reflects the cylindrical form of the micelles. In the case of $(H_3O)_2[C_{12}H_{30}N_2]_3[(UO_2)_4(SeO_4)_8](H_2O)_5$, the inorganic structure forms a strongly undulated sheet, whereas, in the case of **2**, formation of highly porous uranyl selenate nanotubules have been observed (see above). This indicates the possibility of preparation of uranium oxosalt mesostructures if larger organic moieties (e.g., block copolymers) are involved in the synthesis procedure.

4. Conclusions

Actinide peroxide nanospheres [3] and uranyl selenate nanotubules [4,5] represent the first examples of nanoscale structures in inorganic actinide compounds. The nanostructured actinide compounds considered here have been obtained under soft synthesis conditions (room-temperature crystallization from aqueous solutions). Most of these compounds are soluble and it is rather hard to foresee any practical application of them. However, these findings demonstrate the possibility of nanoscale fabrication for actinides in higher oxidation states, and we expect that a whole new range of uranium-based nanotubular and nanocomposite materials can be synthesized. One possible application of these materials is in utilizing depleted U for applications that remain to be discovered, consistent with much of the potential applications of nanomaterials currently being explored in a range of systems.

Acknowledgments

S.V.K. thanks Russian Ministry of Science Education for financial support through the grant RNP 2.1.1.3077 and contract # 02.442.11.7301, and Russian Foundation for Basic Research (grants 06-03-32096, 06-03-97000, and 06-03-42725).

References

[1] C.N.R. Rao, A.K. Cheetham, J. Mater. Chem. 11 (2001) 2887.
[2] C.N.R. Rao, A. Govindaraj, Nanotubes and Nanowires, RSC Publishing, Cambridge, 2005.
[3] P.C. Burns, K.-A. Hughes Kubatko, G. Sigmon, B.J. Fryer, J.E. Gagnon, M.R. Antonio, L. Soderholm, Angew. Chem. Int. Ed. 44 (2005) 2135.
[4] S.V. Krivovichev, V. Kahlenberg, R. Kaindl, E. Mersdorf, I.G. Tananaev, B.F. Myasoedov, Angew. Chem. Int. Ed. 44 (2005) 1134.
[5] S.V. Krivovichev, V. Kahlenberg, R. Kaindl, E. Mersdorf, I.G. Tananaev, B.F. Myasoedov, J. Am. Chem. Soc. 127 (2005) 1072.
[6] Th. Albrecht-Schmitt, Angew. Chem. Int. Ed. 44 (2005) 4836.
[7] P.C. Burns, M.L. Miller, R.C. Ewing, Can. Mineral. 34 (1996) 845.
[8] P.C. Burns, R.C. Ewing, F.C. Hawthorne, Can. Mineral. 35 (1997) 1551.
[9] R. Ma, Y. Bando, T. Sasaki, J. Phys. Chem. B108 (2004) 2115.

[10] A. Muller, F. Peters, M.T. Pope, D. Gatteschi, Chem. Rev. 98 (1998) 239.
[11] A.F. Hebard, M.J. Rosseinsky, R.C. Haddon, D.W. Murphy, S.H. Glarum, T.T.M. Palstra, A.P. Ramirez, A.R. Kortan, Nature 350 (1991) 600.
[12] C.L. Hill, in: M. Ward (Ed.), Comprehensive Coordination Chemistry-II: From Biology to Nanotechnology, vol. 4, Elsevier, Oxford, 2003, p. 679.
[13] J.F. Banfield, H. Zhang, Rev. Mineral. Geochem. 44 (2001) 1.
[14] S.V. Krivovichev, Rev. Mineral. Geochem. 56 (2005) 17.
[15] P.B. Moore, Am. Mineral. 55 (1970) 135.
[16] R. Hoppe, J. Köhler, Z. Kristallogr. 183 (1988) 77.
[17] E. Dvoncova, K.H. Lii, Inorg. Chem. 32 (1993) 4368.
[18] S.V. Krivovichev, S.K. Filatov, T.F. Semenova, Z. Kristallogr. 212 (1997) 411.
[19] V.I. Sokolov, Dokl Akad Nauk 326 (1992) 647.
[20] Y.N. Chiu, J. Xiao, C.D. Merritt, K. Liu, W.X. Huang, P.V. Ganelin, N.N. Li, J. Molec. Struct. TEOCHEM 530 (2000) 67.
[21] S. Iijima, Nature 354 (1991) 56.
[22] G.R. Patzke, F. Krumeich, R. Nesper, Angew. Chem. Int. Ed. 41 (2002) 2446.
[23] L. Krush-Elbaum, D.M. Newns, H. Zeng, V. Derycke, J.Z. Sun, R. Sandstrom, Nature 431 (2004) 672.
[24] S.V. Krivovichev, V.N. Yakovenchuk, T. Armbruster, N. Döbelin, P. Pattison, H.-P. Weber, W. Depmeier, Am. Mineral. 89 (2004) 1561.
[25] S.V. Krivovichev, P.C. Burns, J. Solid State Chem. 170 (2003) 106.
[26] S.V. Krivovichev, V. Kahlenberg, J. Alloys Compd. 389 (2005) 55.
[27] S.V. Krivovichev, V. Kahlenberg, Z. Anorg. Allg. Chem. 630 (2004) 2736.
[28] S.V. Krivovichev, P.C. Burns, Radiochemistry 46 (2004) 408.
[29] S.V. Krivovichev, P.C. Burns, Z. Kristallogr. 218 (2003) 683.
[30] S.V. Krivovichev, P.C. Burns, Z. Kristallogr. 218 (2003) 725.
[31] S.V. Krivovichev, V. Kahlenberg, Z. Anorg. Allg. Chem. 631 (2005) 739.
[32] S.V. Krivovichev, I.G. Tananaev, V. Kahlenberg, B.F. Myasoedov, Radiochemistry 48 (2006) 217.
[33] S.V. Krivovichev, I.G. Tananaev, V. Kahlenberg, B.F. Myasoedov, Radiochemistry 48 (2006) 497.
[34] S.V. Krivovichev, V. Kahlenberg, R. Kaindl, E. Mersdorf, Eur. J. Inorg. Chem. 2005 (2005) 1653.